Soft Matter

Soft Confinement of Self-Propelled Rods: Simulation and Theory

Journal:	*Soft Matter*
Manuscript ID	SM-ART-10-2023-001340.R1
Article Type:	Paper
Date Submitted by the Author:	20-Jan-2024
Complete List of Authors:	Modica, Kevin; University of California Santa Barbara, Chemical Engineering Takatori, Sho; University of California Santa Barbara, Department of Chemical Engineering

Soft Matter

ARTICLE TYPE

Cite this: DOI: 00.0000/xxxxxxxxxx

Soft Confinement of Self-Propelled Rods: Simulation and Theory†

Kevin J. Modica[a] and Sho C. Takatori*[a]

Received Date
Accepted Date

DOI: 00.0000/xxxxxxxxxx

We present an analytical framework for evolving the dynamics of active rods under any periodic external potential, including confining channels and arrays of harmonic traps. As a proof of concept, we analyze the structure and dispersion of self-propelled rods under a soft, periodic one-dimensional (1D) confinement potential and under a two-dimensional (2D) periodic radial harmonic trap. While passive rods and polymers nematically order under 1D confinement, their diffusive transport along the director is limited by thermal diffusion. In contrast, self-propelled rods can generate large convective fluxes when combined with nematic ordering, producing a strong dispersion along the director. Combining theory and simulation, we demonstrate that nematic alignment and self-propulsion generates an exponential enhancement in active diffusivity along the director, in contrast to passive rods that experience at most a 2-fold increase.

1 Introduction

Active rods, characterized by their anisotropic shape and nonequilibrium motion, are a powerful model for describing the behavior of biological constituents across a range of systems, from motile bacteria to cytoskeletal filaments.[1–3] While self-propelled systems are often studied for their collective behaviors, even dilute systems of active particles can present unexpected physics. Despite significant prior work, predicting and controlling the transport and structure of active rods remains an ongoing challenge.

One method to study and control active matter is through geometric confinement.[4–11] Confinement introduces additional complexities to the dynamics of active matter, as interactions with boundaries profoundly influence the emergent properties of the system.[12–20] For active rods, the proportion of normal and parallel alignment to the confinement direction is set by the competition between activity-induced boundary accumulation (normal alignment) and entropy-mediated reorientation (parallel alignment).[21–25]

In addition to impenetrable walls, many systems exhibit a softer form of confinement where escape is made possible (if unlikely) by thermal fluctuations or active forcing. Actin and microtubule filaments placed in shallow channels are known to leave the confining channels when propelled by motor proteins, requiring specific geometries to prevent escape.[26–29] Optical and acoustic tweezers provide another mechanism of weakly confining bacteria and active particles for measuring their motility.[30–32]

Despite the wide prevalence of soft confinement on self-propelled rods, the topic remains under-explored theoretically and in simulation. Existing work on anisotropic colloidal particles uses dynamical density functional theory (DDFT).[33–35] While DDFT has been used to model the mean-field interactions between particles, in the presence of an external field, the user needs to convert the local potential field acting across the mass density of the finite body into a potential energy determined by the particle's center of mass position and orientation.

In this work, we demonstrate a framework for studying dilute active rods in any periodic external field by converting a local potential energy density into a position and orientation dependent potential energy on the rod center of mass. We apply our framework for the special case of a 1D periodic potential to illustrate that soft confinement in channels increases the axial transport even for dilute concentrations of swimmers when the rod length is commensurate to the channel size. Lastly, inspired by optical tweezers, we also apply our framework on a periodic array of harmonic traps to demonstrate the utility of our approach to more complex forms of soft confinement.

2 Model and Methods

In the overdammped limit, the motion of self-propelled rods follows the Langevin equation with no inertia. The rod is treated as a rigid body that propels by an active force directed along the long axis. The active, Brownian, and external forces and torques are summed to generate translational and rotational motion. To simulate a dilute system, the self-propelled rods do not interact with each other (i.e., the rods are "ideal"). The evolution equation for

[a] Department of Chemical Engineering, University of California, Santa Barbara, Santa Barbara, CA 93106 USA; E-mail: stakatori@ucsb.edu

† Electronic Supplementary Information (ESI) available: See DOI: 10.1039/cXsm00000x/

the ith rod's center of mass is:

$$\frac{d\mathbf{r}_i}{dt} = \sqrt{2D_T}\boldsymbol{\eta}_i(t) + \frac{\mathbf{F}_i^{ext}}{\zeta_T} + \frac{\mathbf{F}_i^{act}}{\zeta_T} \tag{1a}$$

$$\frac{d\theta_i}{dt} = \sqrt{2D_\theta}\xi_i(t) + \frac{L_i^{ext}}{\zeta_\theta}. \tag{1b}$$

where ζ_T and ζ_θ are the translational and rotational drag coefficients, $\mathbf{F}_i^{act}$ is the swim force, $\mathbf{F}_i^{ext}$ is the force on the rod center of mass from the external potential, and L_i^{ext} is the torque on the rod center of mass from the external potential. The swim force $\mathbf{F}_i^{act} = U_0\zeta_T\mathbf{u}_i$ is of constant magnitude, with the direction set by the rod orientation unit vector $\mathbf{u}_i = \cos(\theta_i)\hat{\mathbf{e}}_x + \sin(\theta_i)\hat{\mathbf{e}}_y$ in 2D. Finally, the translational and rotational diffusion coefficients are D_T and D_θ, with $(\boldsymbol{\eta}_i,\ \xi_i)$ as random variables with zero mean and a variance consistent with the fluctuation-dissipation theorem.

As a complementary description of the Langevin equation, the probability distribution $f(\mathbf{r},\theta,t)$ of a self-propelled Brownian rod at position $\mathbf{r}$, orientation angle θ and time t confined in 2-dimensions follows the Smoluchowski diffusion equation:

$$\frac{\partial f(\mathbf{r},\theta,t)}{\partial t} + \nabla\cdot\mathbf{J}_T + \frac{\partial}{\partial\theta}J_\theta = 0 \tag{2a}$$

$$\mathbf{J}_T = \left[U_0\mathbf{u}f - \mathbf{D}(\mathbf{u})\cdot\left(\nabla f + f\nabla\left[\frac{V}{k_BT}\right]\right)\right] \tag{2b}$$

$$J_\theta = -D_\theta\left(\frac{\partial}{\partial\theta}f + f\frac{\partial}{\partial\theta}\left[\frac{V}{k_BT}\right]\right). \tag{2c}$$

The Smoluchowski equation can be derived by noise averaging the Langevin equation for the rod.[36,37] It describes the normalized probability density f of rods moving at constant velocity U_0 due to a force acting along its center of mass and oriented along its long axis in direction $\mathbf{u}$. The rods undergo Brownian motion with a (potentially orientationally dependent) translational diffusion tensor $\mathbf{D}(\mathbf{u})$ and rotational diffusion constant D_θ. k_BT is the thermal energy, and V is the potential energy of the entire body in the presence of an external field. $\mathbf{J}_T$ and J_θ represent the translational and angular flux, with the translational gradient operator $\nabla = \frac{\partial}{\partial x}\hat{\mathbf{e}}_x + \frac{\partial}{\partial y}\hat{\mathbf{e}}_y$. For the purpose of this study, interactions between rods are neglected to probe the dilute limit.

When studying anisotropic particles, Eq. 2 is complicated by the calculation of the constituent's potential energy given a potential energy field ϕ and mass distribution ρ

$$V(\mathbf{r},\theta) = \int\phi(\mathbf{r}-\mathbf{s})\rho(\mathbf{s})d\mathbf{s}. \tag{3}$$

The mass distribution ρ is zero everywhere except in the region $\mathbf{r}+\mathbf{s}$ where $\mathbf{r}$ is the rod center of mass, $\mathbf{s} = s\mathbf{u}$ is the displacement along the rod long axis in direction $\mathbf{u}$ from the rod center, with distance spanning from $s = -L_{Rod}/2$ to $s = L_{Rod}/2$ (see Supplementary Information Section I.†).

To find an analytical expression for V, one would traditionally perform a multipole series expansion on ϕ. This Taylor series expansion about the rod center is slow to converge when the potential energy changes rapidly relative to the length of the rod. In fact, a multipole series of a periodic monochromatic field with wavelength λ diverges for $2\pi L_{Rod} \geq \lambda$. To overcome this challenge, we have instead chosen to expand ϕ as a Fourier series and compute the Fourier coefficients (rather than the multipole moments) of $V(\mathbf{r},\theta)$. We compute the convolution in Eq. 3 as a product in Fourier space:

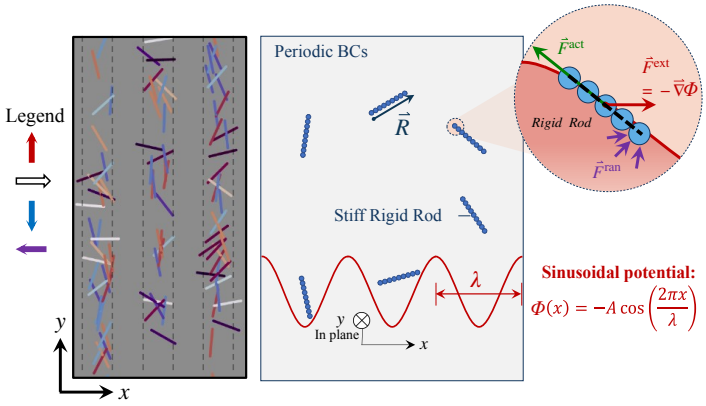

Fig. 1 Schematic of active rods in a monochromatic potential energy field ϕ. The rods are modelled in simulation as a rigid assembly of coarse-grained beads. Left: Simulation snapshot of self-propelled rotors in the potential field, colored by their direction. Right: Schematic demonstrating the rotors are composed of spherical point masses that are pushed by random forces, active forces along the rod contour, and the potential energy field. In all simulations, the rod is composed of 21 coarse-grained beads separated by bond length σ. In the dilute limit, the beads are point masses and do not interact with each other. Therefore, the rod diameter is zero, and the aspect ratio $L_{Rod}/d_{Rod} = \infty$.

$$\hat{V}_{nm}(\theta) = \hat{\phi}_{nm}\hat{\rho}_{nm}(\theta). \tag{4}$$

The Fourier transform of the line density $\hat{\rho}_{nm}$ can be derived analytically as described in Supplementary Information Section I.†, allowing us to determine an expression for the center of mass potential directly:

$$V(\mathbf{r},\theta) = \sum_{n,m}\hat{\phi}_{nm}e^{i2\pi\mathbf{k}_{nm}\cdot\mathbf{r}}\mathrm{sinc}\left(\pi L_{Rod}\mathbf{k}_{nm}\cdot\mathbf{u}\right). \tag{5}$$

The wavevector is defined as $\mathbf{k}_{nm} = \frac{n}{L_x}\hat{\mathbf{e}}_x + \frac{m}{L_y}\hat{\mathbf{e}}_y$. This method converges rapidly for periodic potentials with a low-wavenumber power spectrum. The $\mathrm{sinc}(\pi L_{Rod}\mathbf{k}_{n,m}\cdot\mathbf{u})$ term comes from the Fourier transform of the segment density for a rod[38] and couples the orientation of the rod to the potential energy.

Although Eqs. 2-5 are true for any periodic potential, we will focus on a particular case of active rods confined in a 1D monochromatic potential field as shown in Fig. 1. In this field, the rod potential energy is

$$V(x,\theta) = -A\cos\left(\frac{2\pi x}{\lambda}\right)\mathrm{sinc}\left(\frac{\pi L_{Rod}\cos(\theta)}{\lambda}\right). \tag{6}$$

We compare the solutions to the Smoluchowski equations to discrete simulations of thin rods using Brownian dynamics (BD) simulations. The rods are composed of coarse-grained beads separated by distance σ connected by rigid body constraints. Each bead on the rigid rod feels the potential energy field ϕ, and the resultant forces and torques move the rod center of mass and ro-

tate the body. The center of mass potential energy in this discrete system is slightly modified from the continuum limit (see Supplementary Information Section I.†), but Eq. 5 is suitable within error for our results when $L_{Rod}/\sigma \gtrsim 10$. For the following results, we set $L_{Rod}/\sigma = 21$. As mentioned in Fig. 1, this study is focused on dilute systems and as such the coarse-grained beads are point masses that have no interparticle interactions. Therefore, the rod diameter is zero, and the aspect ratio $L_{Rod}/d_{Rod} = \infty$.

Based on the form of the external potential, and ignoring any directional dependence to the translational drag $D_{\parallel} \approx D_{\perp} = D_T$, there are four dimensionless groupings present in the system: the ratio of rod length to the confinement wavelength L_{Rod}/λ, the ratio of active run length to the rod length $U_0/(D_\theta L_{Rod})$, the translational diffusivity over the rotational diffusivity $D_T/(D_\theta L_{Rod}^2)$, and the trap strength divided by the thermal energy $A/(k_B T)$. For all systems discussed, we choose $D_T/(D_\theta L_{Rod}^2) = 1/6$, following the traditional scaling of rotational diffusion for a thin rod in dilute conditions.[37]

In addition to solving the steady state Smoluchowski equation in a periodic unit cell, we utilize the mechanics of generalized Taylor dispersion theory to calculate the long-time self-diffusivity of the dilute rods in confinement.[39–41] For brevity, we save the mechanics of the derivation and solution to the dispersion equations for Supplementary Information Section II.†.

We implemented our simulations using HOOMD-blue, a molecular dynamics (MD) simulation package in Python.[42] We integrate the Langevin equation using a timestep size of $\Delta t = 0.01\sigma^2/D_T$ for at least $2 * 10^7$ timesteps. Numerical solutions to the field equations were conducted using spectral methods implemented in Dedalus.[43]

3 Results and Discussion

To compare the effect of confinement on passive and active rods, we plot the component of the normalized nematic tensor aligned orthogonal to the external field $\langle Q_{yy} \rangle$ in Fig. 2 a) and b). The angled brackets indicate the ensemble average of the quantity over all particles and timesteps ($N_{samples}$) for BD simulations. For the solutions to the Smoluchowski equation, the angled brackets indicate the expected value calculated by integrating the probability distribution.

$$\langle Q_{yy} \rangle_{sim} = \frac{1}{N_{samples}} \sum_{i}^{N_{samples}} \left(2\sin^2(\theta_i) - 1 \right) \tag{7a}$$

$$\langle Q_{yy} \rangle_{theory} = \iint_{\mathbf{r},\theta} f(\mathbf{r},\theta)(2\sin^2(\theta) - 1)\mathrm{d}\mathbf{r}\mathrm{d}\theta \tag{7b}$$

These values are equivalent at steady state.

As the potential strength $A/(k_B T)$ increases, the rods experience an aligning torque due to their finite length. The potential energy is minimized when all monomers on the rod are located at $x = 0$; therefore, energy is minimized at the expense of rotational entropy by the rotation of the entire rod. In addition to large potential strengths ($A \gg k_B T$), Q_{yy} is maximized when the rod length increases relative to the wavelength; the energy penalty increases as more of the rod density is moved further from the potential energy minimum. Both active and passive rods exhibit

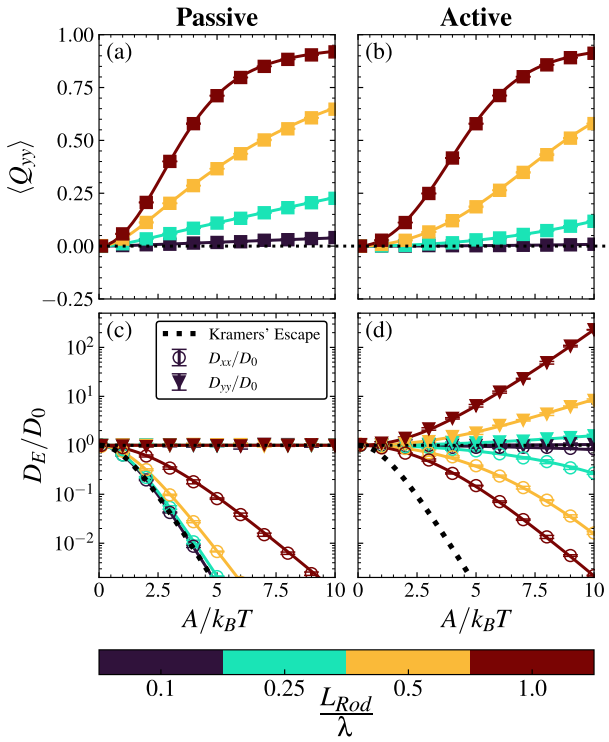

Fig. 2 Softly confined active rods exhibit significant nematic ordering and dispersion in a direction orthogonal to confinement. Panels (a) and (c) are passive whereas panels (b) and (d) are self-propelled rods with activity $U_0/(D_\theta L_{Rod}) = 3.5$. Panels (a) and (b) show the axial component of the traceless ensemble averaged nematic tensor. Panels (c) and (d) show the components of the effective diffusivity scaled by the bulk diffusivity in the absence of confinement. While the diffusivity across confining channels (D_{xx}/D_0) decreases for both active and passive rods, the active rods exhibit enhanced diffusivity in the direction orthogonal to confinement (D_{yy}/D_0) as rod length and field strength increase. Markers are from Brownian dynamics simulations, solid lines are numerical solutions to the Smoluchoski and dispersion theories. Error bars are standard error of the mean calculated from three independent simulations and when not visible are smaller than the marker size. Dotted lines in panels (c) and (d) are the Kramers' escape solution for diffusivity of a point particle.

increased nematic ordering as the field strength and rod length increase. Compared to the passive rods, self-propelled rods at the activity studied exhibit slightly less nematic order at the same trap strength due to their increased ability to escape the trap basin and reorient at a more favorable location.

In Fig. 2 c) and d), we calculate the long time self diffusivity of the confined active rods scaled by the bulk diffusivity in the absence of external fields, D_E/D_0. The bulk diffusivity, $D_0 = D_T + U_0^2/(2D_\theta)$, is defined as the sum of the Stoke-Einstein-Sutherland diffusivity D_T and the "swim diffusivity" $U_0^2/(2D_\theta)$ for active species. In the absence of confinement $D_E = D_0$. This normalization isolates the impact of the activity-confinement coupling, instead of capturing the well studied enhancement in bulk diffusivity due to activity.

We plot the components of the diffusivity aligned with the external field, D_{xx}/D_0, and orthogonal to the external field, D_{yy}/D_0, for passive and active rods. For passive rods, D_{xx}/D_0 decreases following a standard Kramers' escape process (dashed black line).

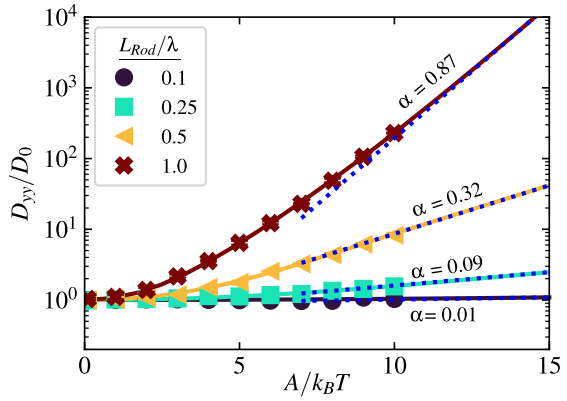

Fig. 3 1D monochromatic potentials increase active rod dispersion orthogonal to confinement by preventing reorientation. As rod length increases, the activation barrier against rotation grows. Data points are measured from Brownian dynamics simulations and the solid lines are numerical solutions to the full dispersion theory. The dotted lines are predictions from Eq. 8 with n=2. Activity $U_0/(D_\theta L_{Rod}) = 3.5$ Error bars are from three independent simulations and when not visible are smaller than the marker size.

Kramers' theory[44–46] indicates that the effective diffusivity scales linearly with the curvature of the potential well and exponentially with the activation energy barrier to hopping. Note that when the rod length is comparable to the wavelength $L_{Rod}/\lambda = 1$, the scaled diffusivity is slightly higher due to the coupling between the density and higher order moments (e.g. nematicity) from the potential. Long rods near the top of the trap are able to reorient so that part of their mass density is in the next basin, creating a weaker activation barrier to escape. In contrast, the scaled dispersivity perpendicular to the field D_{yy}/D_0 remains unaffected by confinement. Transport in the axial direction follows a 1D random walk at its bulk diffusivity $D_{yy} = D_0$. For the purpose of this work, we ignored any orientation dependence to the Stokes-Einstein-Sutherland diffusivity, but at most that would modify the results by a factor of two for an infinitely long and thin rod.

For active rods in Fig. 2 d), the effective diffusivity between channels (D_{xx}/D_0) decreases as rod length increases. The active forcing is powerful enough to overcome the external field in all cases $F^{act}/F^{ext}_{max} = (U_0 k_B T/D_T)/(A/\lambda) > 1$; however, the large nematic order present as L_{Rod}/λ increases prevents reorientation and inhibits facilitated active escape.

Most surprisingly, the axial diffusivity of active rods in confinement increases by many orders of magnitude such that $D_{yy}/D_0 \gg 1$. Rod alignment via the external potential couples with persistent self-propulsion to increase the dispersion. At strong field strengths and long rod lengths, the rods align nematically inside the channel field, moving ballistically until an energetically unlikely reorientation effect occurs. The time between direction reversals is increased by the potential barrier, leading to exponentially longer ballistic runs.

To understand the cause of the increase in dispersion, we can examine the energetics of direction reversal for confined rods. At strong field strengths, $A \gg k_B T$, the rod number density is focused primarily in the center of the channel. A rod sitting in the center oriented vertically ($\theta = \pi/2$) has an activation energy barrier to change direction to $\theta = 3\pi/2$, which for $L_{Rod}/\lambda \leq 1$ is the energy needed to rotate through the completely horizontal state: $E_{a,rot} = A\left[1 - \mathrm{sinc}\left(\frac{\pi L_{Rod}}{\lambda}\right)\right]$. This activation energy determines the frequency of direction reversal. The activation barrier exponentially lowers the effective *rotational* diffusion coefficient ($D_{E,\theta}$); however, due to the coupling between orientation and persistent self-propulsion, the reduced rotational diffusion increases the effective translational diffusion.

We propose that when the rod is strongly confined, the effective translational diffusivity of an active rod in an external potential may be approximated as

$$D_{E,yy}/D_0 \sim e^{\alpha} \approx e^{nE_{a,rot}/k_B T}, \tag{8}$$

where $E_{a,rot}$ is the activation barrier to for the rod to rotate and reverse polarity. And n is a factor depending weakly on rod length. Over the course of our study, we found $n \approx 2$, but it is not necessarily constant for all systems.

In Fig. 3), we compare the effective diffusivity from our Brownian dynamics simulations (via slope of the mean-squared displacement) with our proposed theoretical model in Eq. 8. When confinement strength is weak ($A \ll k_B T$), the effective diffusivity is equivalent to the bulk diffusivity. As the confinement strength increases to $A \gg k_B T$, the effective diffusivity increases exponentially, based on the formation of an activation barrier to rotation $D_{E,yy} \sim 1/D_{E,\theta} \sim e^{\alpha}$. Across an order of magnitude of rod lengths, we obtain proficient agreement between the simulation data and our proposed theoretical model, Eq. 8.

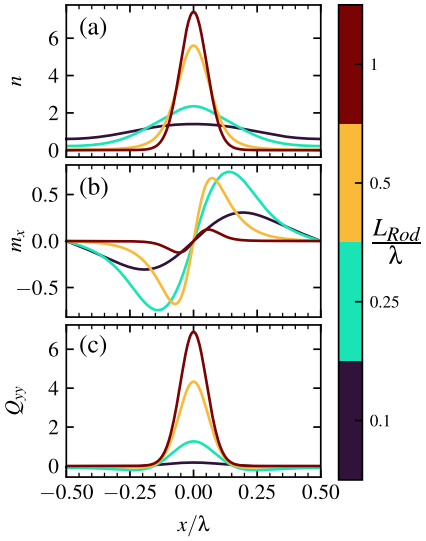

Fig. 4 Steady state moments of the probability distribution found numerically via Eq. 2 for a 1D monochromatic potential $\phi = -A\cos(2\pi x/\lambda)$. Active rods at potential strength $A/(k_B T) = 10$ and activity $U_0/(D_\theta L_{Rod}) = 3.5$. (a) Rod number density (n) across the channel increases due to the large nematic preventing active escape. (b) Rod polar order against the channels (m_x) exhibits a maximum at intermediate L_{Rod}/λ because the maximum restoring force (A/λ) and active force balance before succumbing to nematic reorientation. (c) Rod nematic order in the channels (Q_{yy}) increases as L_{Rod}/λ grows due to the increased barrier to reorientation.

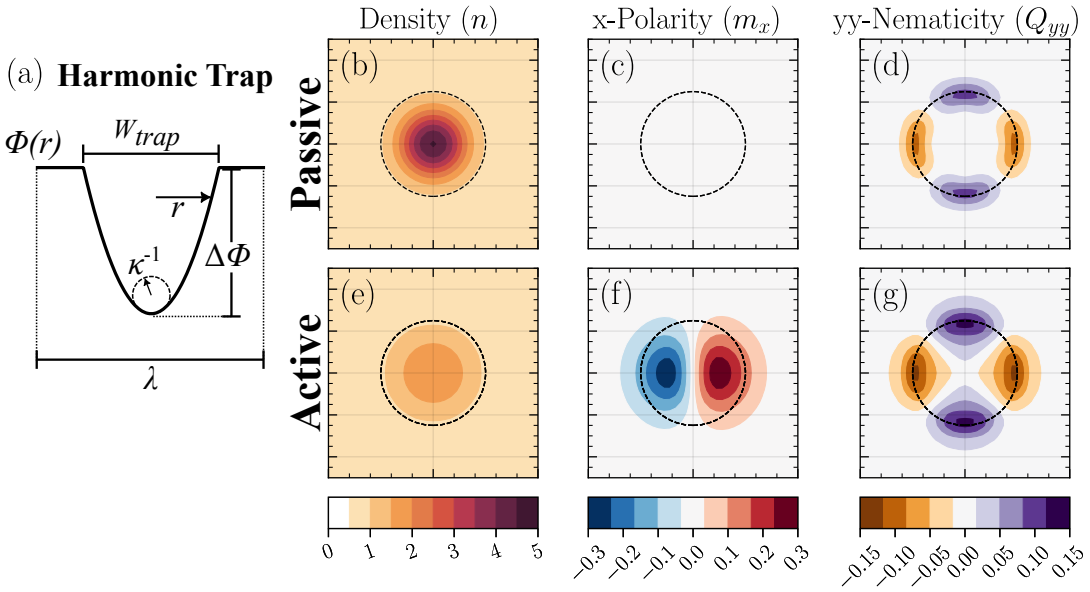

Fig. 5 (a) An optical trap potential energy field $\phi(r)$ defined as a radially harmonic trap with curvature κ, width W_{trap} and depth $\Delta\phi = \frac{1}{8}\kappa W_{trap}^2$. (b)-(g) Moments of the steady-state probability distribution for rods in an array of optical traps in two dimensions. Upper panels (b,c and d) are for passive (not self-propelled) rods in a harmonic trap, lower panels (e,f and g) are for self-propelled rods with activity set as $U_0/(D_\theta L_{Rod}) = 1.0$. Panels (b) and (e) are the number density of rods, center panels (c) and (f) are the polar order of rods in the x-direction, and bottom panels (d) and (g) are the nematic order in the y-direction. The circular dashed line represents the edge of the trap. The trap width $W_{trap} = 0.5\lambda$ and trap depth $\Delta\phi = 2k_BT$ gives a curvature $\kappa = 64\lambda^{-1}$. For this example, rod length $L_{Rod} = 0.25\lambda$.

Our Smoluchowski formulation allows for a detailed view of the local rod structure found via the probability distribution. In Fig. 4a) - c), we calculate the local density, polarity, and nematicity fields across a single channel at a fixed potential strength of $A/(k_BT) = 10$. The local density ($n(x) = \iint f(x,y,\theta)\mathrm{d}y\mathrm{d}\theta$) increases as L_{Rod}/λ increases. For low L_{Rod}/λ, the active force is easily able to overcome the potential energy barrier and there is a broad density distribution. At large L_{Rod}/λ, the small wavelengths lead to large gradients of the potential energy creating a restoring force similar in magnitude to the active force $A/\lambda \approx 0.48U_0(k_BT/D_T)$ (for $L_{Rod} = \lambda$). Additionally, the strong torques at large L_{Rod}/λ prevents rod orientation (and therefore self-propulsion) out of the basin.

Interestingly, the polarity in the x-direction ($m_x(x) = \iint f(x,y,\theta)\cos(\theta)\mathrm{d}y\mathrm{d}\theta$) increases non-monotonically as a function of wavelength. When L_{Rod}/λ is small, the aligning torques on the rods are weak, and the self-propelled rods behave as active spheres, orienting against restoring forces. The polarity should increase with the restoring force, but eventually the torques on the rods dominate and prevent alignment with the x-axis (normal to the soft confinement). Finally, the nematic order ($Q_{yy}(x) = \iint f(x,y,\theta)(2\sin^2(\theta)-1)\mathrm{d}y\mathrm{d}\theta$) increases with L_{Rod}/λ as large gradients in potential energy along a single filament length rotate the particle.

Although we focused on the special case of a 1D sinusoidal potential, our spectral formulation (Eq. 5) is universal for any well behaved periodic potential energy field. To demonstrate the application of our framework towards more complex potentials, we solved the steady-state probability distribution of a rod in a lattice array of radially parabolic potentials, inspired by an array of optical traps.[41] Optical traps do not necessarily have a parabolic profile for anisotropic colloidal particles[47]; however, this model provides a useful demonstration of the range of energy fields made possible to study.

In Fig. 5a), we show a schematic of a parabolic potential described by the trap curvature κ, width W_{trap} and depth $\Delta\phi = \frac{1}{8}\kappa W_{trap}^2$. This parabolic trap biases the rod density to the center, but may also impact the (local) polarity and nematicity of the rods, especially with activity. We cut off the parabolic potential at the width W_{trap} to create a finite activation barrier to escape, we then tile the potential in a square lattice to measure properties of the entire suspension as opposed to motion within a single stiff trap. In Fig. 5b)-g), we show the density, x-direction polarity, and yy-direction nematicity for both passive and self-propelled rods, respectively. In Fig. 5b) and e), the number density is maximized at the center of the trap. However, the addition of activity allows for particles to more easily escape from the harmonic trap, as previously shown for spherical active particles.[31,48–51]

Self-propulsion adds an orientation-dependent force to the translational flux, thereby coupling the polar order to potential and concentration gradients in a way not present for passive rods. As shown in Fig. 5c) and f), this coupling generates local polar order from the propulsive force “pushing" against the energy barrier, which corresponds to a maxima in polar order in locations where the potential energy gradient is the strongest.

The isotropic nature of the trap prevents global orientational ordering vertically or horizontally; however, the rods will tend to align in such a way that they “hang" over the edge, thereby lowering their potential energy. This creates the quadrupolar structure present in Fig. 5d) and g). This effect is modified for active parti-

cles because the polar order induced by pushing against the trap feeds into the local nematic order in regions of high restoring force.

4 Conclusions

This work presents a general method to study anisotropic active rods in two dimensions under a range of periodic external fields. Extensions to this work include the study of rods in three dimensional confinement, where the Fourier transform of the rod density ($\mathrm{sinc}(\pi L_{Rod}\mathbf{k}_{n,m}\cdot\mathbf{u})$) remains the same provided that $\mathbf{u}$ is now the unit vector in spherical coordinates.

Extending this work to concentrated suspensions of active rods is possible using a modification to the Smoluchowski equation to incorporate a mean-field model.[37,52,53] However, mean-field models are only valid in the regime of low rod density, weak interparticle interactions, and small density correlations, so phenomenological hydrodynamic models are often used to study concentrated active nematic systems.[53] For example, recent theoretical work by Gulati et. al.[54] on concentrated suspensions of polar fluids confined between walls demonstrates that by controlling the wall anchoring and the activity, one can transition between no flow, laminar, shear banded, and vortex lattice flow types. We believe that the machinery of Eq. 5 can also extend these phenomenological methods by enabling the addition of a variety of periodic potentials to rod models.

Conflicts of Interest

There are no conflicts of interest to declare.

Acknowledgements

We wish to acknowledge Dr. Joseph Barakat for helpful discussions that in part inspired this work and for his mentorship in implementing numerical and analytical methods in practice for studying interesting transport problems. Research was sponsored by the U.S. Army Research Office and accomplished under cooperative agreement W911NF-19-2-0026 for the Institute for Collaborative Biotechnologies. K.J.M. is supported by the National Science Foundation Graduate Research Fellowship under Grant No. 1650114. S.C.T. is supported by the Packard Fellowship in Science and Engineering. Use was made of computational facilities purchased with funds from the National Science Foundation (CNS-1725797) and administered by the Center for Scientific Computing (CSC). The CSC is supported by the California NanoSystems Institute and the Materials Research Science and Engineering Center (MRSEC; NSF DMR 2308708) at UC Santa Barbara.

Notes and references

1 A. Be'er and G. Ariel, *Movement Ecology*, 2019, **7**, 9.
2 M. Bär, R. Großmann, S. Heidenreich and F. Peruani, *Annual Review of Condensed Matter Physics*, 2020, **11**, 441–466.
3 S. J. Kron and J. A. Spudich, *Proceedings of the National Academy of Sciences*, 1986, **83**, 6272–6276.
4 R. Voituriez, J. F. Joanny and J. Prost, *Europhysics Letters (EPL)*, 2005, **70**, 404–410.
5 H. Wioland, F. G. Woodhouse, J. Dunkel, J. O. Kessler and R. E. Goldstein, *Phys. Rev. Lett.*, 2013, **110**, 268102.
6 E. Lushi, H. Wioland and R. E. Goldstein, *Proceedings of the National Academy of Sciences*, 2014, **111**, 9733–9738.
7 K.-T. Wu, J. B. Hishamunda, D. T. N. Chen, S. J. DeCamp, Y.-W. Chang, A. Fernández-Nieves, S. Fraden and Z. Dogic, *Science*, 2017, **355**, eaal1979.
8 S. Chen, P. Gao and T. Gao, *Journal of Fluid Mechanics*, 2017, **835**, 393–405.
9 A. Opathalage, M. M. Norton, M. P. N. Juniper, B. Langeslay, S. A. Aghvami, S. Fraden and Z. Dogic, *Proceedings of the National Academy of Sciences*, 2019, **116**, 4788–4797.
10 Z. You, D. J. G. Pearce and L. Giomi, *Science Advances*, 2021, **7**, 10694.
11 C. G. Wagner, M. M. Norton, J. S. Park and P. Grover, *Phys. Rev. Lett.*, 2022, **128**, 028003.
12 A. Doostmohammadi, J. Ignés-Mullol, J. M. Yeomans and F. Sagués, *Nature Communications*, 2018, **9**, 3246.
13 D. Needleman and Z. Dogic, *Nature Reviews Materials*, 2017, **2**, 17048.
14 C. Bechinger, R. D. Leonardo, H. Löwen, C. Reichhardt, G. Volpe and G. Volpe, *Reviews of Modern Physics*, 2016, **88**, 045006.
15 S. P. Thampi, *Current Opinion in Colloid & Interface Science*, 2022, **61**, 101613.
16 K. J. Modica, A. K. Omar and S. C. Takatori, *Soft Matter*, 2023, **19**, 1890–1899.
17 J. Elgeti and G. Gompper, *EPL (Europhysics Letters)*, 2013, **101**, 48003.
18 Y. Fily, A. Baskaran and M. F. Hagan, *Soft Matter*, 2014, **10**, 5609–5617.
19 F. Smallenburg and H. Löwen, *Phys. Rev. E*, 2015, **92**, 032304.
20 W. Yan and J. F. Brady, *Soft Matter*, 2018, **14**, 279–290.
21 H. H. Wensink and H. Löwen, *Physical Review E*, 2008, **78**, 031409.
22 J. Elgeti and G. Gompper, *EPL (Europhysics Letters)*, 2009, **85**, 38002.
23 G. Li and J. X. Tang, *Phys. Rev. Lett.*, 2009, **103**, 078101.
24 A. Zöttl and H. Stark, *Journal of Physics: Condensed Matter*, 2016, **28**, 253001.
25 Z. Wang, Y.-F. Chen, H.-Y. Chen, Y.-J. Sheng and H.-K. Tsao, *Soft Matter*, 2018, **14**, 2906–2914.
26 J. Clemmens, H. Hess, J. Howard and V. Vogel, *Langmuir*, 2003, **19**, 1738–1744.
27 J. Clemmens, H. Hess, R. Lipscomb, Y. Hanein, K. F. Böhringer, C. M. Matzke, G. D. Bachand, B. C. Bunker and V. Vogel, *Langmuir*, 2003, **19**, 10967–10974.
28 R. Bunk, J. Klinth, L. Montelius, I. A. Nicholls, P. Omling, S. Tågerud and A. Månsson, *Biochemical and Biophysical Research Communications*, 2003, **301**, 783–788.
29 R. Bunk, M. Sundberg, A. Månsson, I. A. Nicholls, P. Omling, S. Tågerud and L. Montelius, *Nanotechnology*, 2005, **16**, 710–717.
30 A. Ashkin and J. M. Dziedzic, *Science*, 1987, **235**, 1517–1520.

31 S. C. Takatori, R. De Dier, J. Vermant and J. F. Brady, *Nature Communications*, 2016, **7**, 10694.

32 T. L. Min, P. J. Mears, L. M. Chubiz, C. V. Rao, I. Golding and Y. R. Chemla, *Nature Methods*, 2009, **6**, 831–835.

33 H. H. Wensink, H. Löwen, M. Marechal, A. Härtel, R. Wittkowski, U. Zimmermann, A. Kaiser and A. M. Menzel, *The European Physical Journal Special Topics*, 2013, **222**, 3023–3037.

34 R. Wittkowski and H. Löwen, *Molecular Physics*, 2011, **109**, 2935–2943.

35 H. Hansen-Goos and K. Mecke, *Phys. Rev. Lett.*, 2009, **102**, 018302.

36 A. Baskaran and M. C. Marchetti, *Phys. Rev. E*, 2008, **77**, 011920.

37 M. Doi and S. F. Edwards, *The Theory of Polymer Dynamics (International Series of Monographs on Physics)*, Oxford University Press, 1988.

38 M. Doi, T. Shimada and K. Okano, *The Journal of Chemical Physics*, 1988, **88**, 4070–4075.

39 J. F. Morris and J. F. Brady, *Journal of Fluid Mechanics*, 1996, **312**, 223–252.

40 R. N. Zia and J. F. Brady, *Journal of Fluid Mechanics*, 2010, **658**, 188–210.

41 J. M. Barakat and S. C. Takatori, *Physical Review E*, 2023, **107**, 014601.

42 J. A. Anderson, J. Glaser and S. C. Glotzer, *Computational Materials Science*, 2020, **173**, 109363.

43 K. J. Burns, G. M. Vasil, J. S. Oishi, D. Lecoanet and B. P. Brown, *Phys. Rev. Res.*, 2020, **2**, 023068.

44 H. Kramers, *Physica*, 1940, **7**, 284–304.

45 H. Brinkman, *Physica*, 1956, **22**, 29–34.

46 H. Brinkman, *Physica*, 1956, **22**, 149–155.

47 J. L. Abbott, J. A. Spiers, Y. Gao, D. G. A. L. Aarts and R. P. A. Dullens, *Journal of Physics D: Applied Physics*, 2019, **52**, 024002.

48 A. Pototsky and H. Stark, *EPL (Europhysics Letters)*, 2012, **98**, 50004.

49 A. Geiseler, P. Hänggi and G. Schmid, *The European Physical Journal B*, 2016, **89**, 175.

50 D. Wexler, N. Gov, K. O. Rasmussen and G. Bel, *Phys. Rev. Res.*, 2020, **2**, 013003.

51 E. Woillez, Y. Kafri and N. S. Gov, *Phys. Rev. Lett.*, 2020, **124**, 118002.

52 A. Baskaran and M. C. Marchetti, *Phys. Rev. Lett.*, 2008, **101**, 268101.

53 M. C. Marchetti, J. F. Joanny, S. Ramaswamy, T. B. Liverpool, J. Prost, M. Rao and R. A. Simha, *Rev. Mod. Phys.*, 2013, **85**, 1143–1189.

54 P. Gulati, S. Shankar and M. C. Marchetti, *Frontiers in Physics*, 2022, **10**, 1.